Growth of MoS_2 Thin Films with Microdome Texture as Omnidirectional Light Trap for Solar Cell Applications

Hussain M. Abouelkhair[1], Nina A. Orlovskaya[2], and Robert E. Peale[1]

[1]Department of Physics, University of Central Florida, Orlando, Florida, 32816, United States

[2]Department of Mechanical & Aerospace Engineering, University of Central Florida, Orlando, Florida, 32816, United States

***Abstract* — Antireflection by microdome texture on MoS2 thin films is reported. MoS2 films with uniformly distributed microdomes were grown by atmospheric pressure chemical vapor deposition, with structure and composition confirmed by Raman, x-ray diffraction, and energy dispersive x-ray analysis. The morphology and distribution of the domes were investigated by scanning electron microscopy. Finite difference time domain simulations of reflectance show that parabolic domes of 0.5 µm base diameter and 1 µm height can eliminate reflection for incidence angles up to 50°, which can improve light harvesting and efficiency of MoS2-based solar cells.**

***Index Terms* — antireflection microdomes, chemical vapor deposition, molybdenum disulfide, Raman spectroscopy, scanning electron microscopy, solar cells, x-ray diffraction**

I. Introduction

Light harvesting of incident light on solar cells is critical for boosting their efficiency. A 33% reflectance means we lose one third of the incident light energy. Minimizing this reflectance to zero would increase the efficiency by 50% if all the absorbed photons generate hole-electron pairs that are collected. Two techniques are known to reduce reflections. The first is smooth antireflection coatings, which strongly reduce reflectance at a specific wavelength and for a narrow range of light incident angles by destructive interference [1]-[3]. The second is engineered micro- or nano-structures on the front surface of solar cells [4]-[6], which advantageously feature broad spectral range and omnidirectionality in comparison with the smooth coatings [5]-[9]. For such antireflection structures, three main geometries have been studied, namely pyramids [6, 10-14], domes [5], [8], [9], [15]-[17], and pillar [18]-[22]. Nanotips, nanocones, and nanowires can be considered special cases of the basic shapes by considering elongation in one direction. The usual Fresnel reflection due to the sudden refractive index discontinuity is decreased or almost eliminated by the surface structures, which gradually change the effective refractive index between the two media [23]. Inspiration comes from the dome structures on the corneal surface of moths' eyes, which efficiently suppress reflectance for better light-harvesting and night vision [15], [17], [23]-[26]. The optimum structure geometries depend on the materials considered, while ease of fabrication depends strongly on the specific shapes. Thus, experimentally optimizing for structure shape is impractical. Simulating these structures using rigorous three-dimensional finite difference time domain (3D-FDTD) method facilitates the study and optimization of structures geometries.

MoS_2 is one of the promising materials for solar cells due to its favorable optical, electrical, chemical, and mechanical properties [27]-[29]. MoS_2 absorption coefficient ~ 10^5 cm^{-1} exceeds that of silicon [28], [29], potentially allowing thinner, lighter, and cheaper solar cells. The bandgap of MoS_2 is 1.3 eV, which matches well the solar spectrum. The predicted high mobility (410 cm^2 V^{-1} s^{-1}), mechanical flexibility and the chemical inertness to most acids of MoS_2 have attracted the attention [30]. On the other hand, MoS_2 has high refractive index ~ 3.5 which causes 31% reflection loss for light normally incident on its smooth surface [31]. Therefore front-surface antireflection structures are essential to maximize light harvesting and minimize losses [8].

Here we investigate different anti-reflection structure geometries on a smooth film of MoS_2 for solar cell applications. This study is relevant to MoS_2 films with microdome texture, which we grew by atmospheric pressure chemical vapor deposition. The microdomes which appear spontaneously without any lithographic processing are shown to be effective as an omnidirectional light trap. The demonstrated method of growth has significance for MoS_2-based solar cells and other optical and optoelectronic applications.

II. Simulation

Microdomes of MoS_2 on a smooth film of MoS_2 supported by sapphire substrate were simulated and analyzed using the 3D-FDTD method to determine the best structure geometry and arrangement that results in minimum reflectance at different angles and broad spectrum. The incident light source was a plane wave with either S or P polarization. The reflectance from unpolarized light source was calculated as follows:

$$\langle |E|^2 \rangle = \frac{1}{2}|\bar{E}_s|^2 + \frac{1}{2}\left|\bar{E}_p\right|^2 \quad (1)$$

Where $<|E|^2>$ represents the time-averaged electric field intensity of an unpolarized beam light source. $|\bar{E}_s|^2$and $\left|\bar{E}_p\right|^2$

represents the reflectance from S and P polarized light source respectively. Bloch boundaries were used vertically and perfectly matched layers (PML) boundaries were used horizontally above the domes and below the substrate. The wavelength dependence of refractive index and extinction coefficient of the domes, the film and, the substrate was considered in the simulation. We used the FDTD software (Lumerical Solutions, Inc.) to calculate total reflectance (specular plus diffuse) for different shapes and geometries.

Parameters that affect reflectance include dome base diameter, height, and spatial distribution on the surface. We first investigated the effect of different base diameters on reflectance using monochromatic incident light with 500 nm wavelength, which corresponds to the peak of the solar spectrum [8]. The best base diameter that minimized reflectance was then considered in simulations at different wavelengths from 300 to 1200 nm. The effect of height and distribution have been investigated as well.

III. Experimental

MoS_2 was grown by a two-step process. First, a 100 nm molybdenum thin film was electron-beam evaporated on a pre-cleaned c-plane sapphire wafer. Second, the molybdenum film was sulfurized in a two-zone atmospheric pressure chemical vapor deposition (APCVD) system, which is illustrated schematically in Fig. 1.

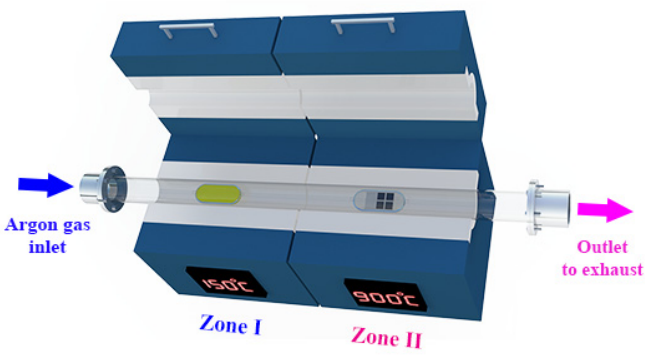

Fig. 1. Schematic illustration of a two-zone APCVD setup.

The sulfur powder (Sigma-Aldrich purum ≥ 99.5%) was placed in the middle of the first zone (150 °C), and the Mo film was placed face-up in the middle of the second zone (900 °C). Ultrahigh pure argon carried sulfur vapor to the growth zone at a rate of 24 sccm/min. Once the second zone reaches 900 °C, it was kept for 30 minutes (sample A) or 60 minutes (sample B) at this temperature, then cooled down to room temperature at a rate of 20 °C/min.

Raman spectroscopy was carried out at room temperature using a Renishaw's inVia micro-Raman spectrometer system with 532 nm 100 mW laser excitation. The laser spot size was 1–2 µm. X-ray diffraction (XRD) was performed using a PANalytical X'Pert^3 MRD X-ray diffractometer with a hybrid monochromator source, operating at 45 kV and 40 mA. The surface morphology of as-grown MoS_2 thin films was characterized by a Zeiss ULTRA-55 FEG scanning electron microscope (FEG-SEM). The composition was analyzed by an energy dispersive x-ray analyzer (EDX) coupled to the FEG-SEM. The total reflectance (specular plus diffuse) measurements were performed using LABSPHERE integrating sphere attached to CARY 500 spectrophotometer.

IV. Results And Discussion

A. Simulation

Fig. 2 shows the total reflectance of parabolic domes with different base diameters. The square array of domes is on a 2.5-µm-thick smooth film of MoS_2 supported by a sapphire substrate. Each reflectance point in the plot represents the average reflectance over all light incident angles from 0° to 80°. This demonstrates the omnidirectionality of these structures. The domes height is half the diameter in all cases. The incident light wavelength is 500 nm.

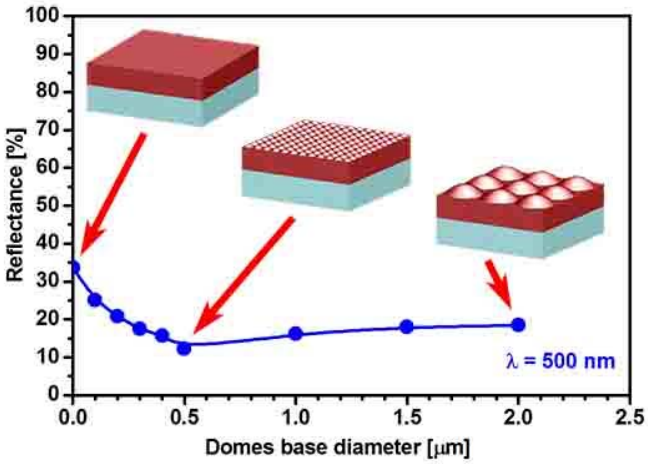

Fig. 2. The reflectance of MoS_2 domes with different base diameters.

The reflectance decreases from 33.6% to 12.2% with increasing the base diameter from 0 to 0.5 µm. Then the reflectance slightly increases to 18.5% with increasing the diameter from 0.5 µm to 2 µm. Therefore we chose the 0.5 µm diameter for further studies over a broad range of wavelengths. As shown in Fig. 2 the most effective base diameter equals the incident wavelength, but we next demonstrate that the same base diameter is nearly equally effective at all relevant wavelengths.

Fig. 3 shows a comparison between the reflectance of a smooth film and 0.5 µm diameter domes over a broad range of wavelengths from 300 nm to 1200 nm. Each reflectance point in the plot represents the average reflectance over all light

incident angles from 0° to 80°. The reflectance decreased by 51% over the whole range. This demonstrates the broad spectral range for the effectiveness of these structures. The wavelength independence of reflectance reinforces the effective medium theory [32] and shows that the antireflection effect is due the gradual change of effective refractive index rather than scattering.

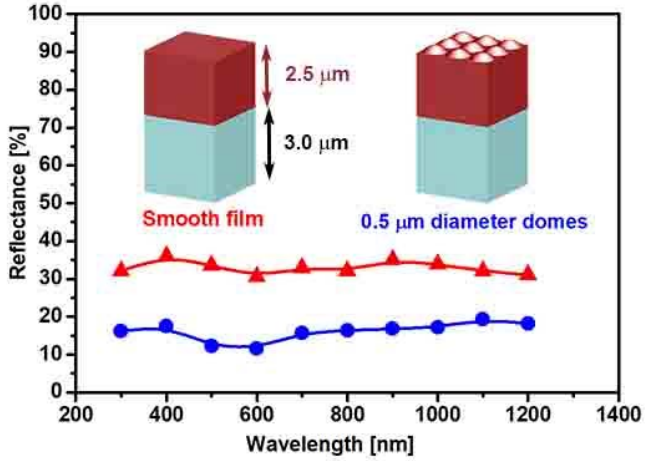

Fig. 3. The reflectance of a square array of MoS_2 domes with 0.5 μm base diameter compared to that of the smooth film.

Fig. 4 shows the reflectance of square arrays of parabolic domes with different heights but constant 0.5 μm base diameter.

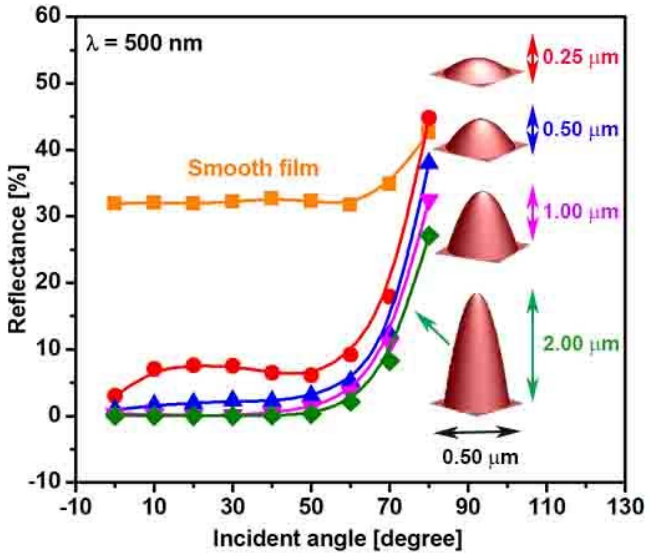

Fig. 4. The reflectance of square arrays of MoS_2 parabolic domes with different heights. The domes base diameter is 0.5 μm for all heights.

The total (specular plus diffuse) reflectance averaged over all the incident angles from 0° to 80° decreased from 12.18% to 4.22% as the height of the dome increased from 0.25 μm to 2 μm. Importantly, the average reflectance of domes with heights 1 μm and 2 μm is practically zero over all the incident light angles from 0° to 50°.

Fig. 5 shows the reflectance averaged over incident angles from 0° to 80° for different spatial distributions of domes and monochromatic incident light with 500 nm wavelength. The hexagonal array of parabolic domes with 0.5 μm base diameter and 0.25 μm height reduces the reflectance more efficiently than a square array of these domes, but this effect is less than the difference in fill factors: For the square array of parabolic domes, the fill factor is 39%, while for the hexagonal array it is 45%. In addition, we compared the former two arrays to hexagonal arrays of pyramids, cones, and hemispherical domes of the same base area and height. The average reflectance of the pyramids was the highest while the hexagonal array of parabolic domes was lowest. Cones had the second highest reflectance after the pyramids. Thus smooth structures such as domes are better than faceted structures such as pyramids.

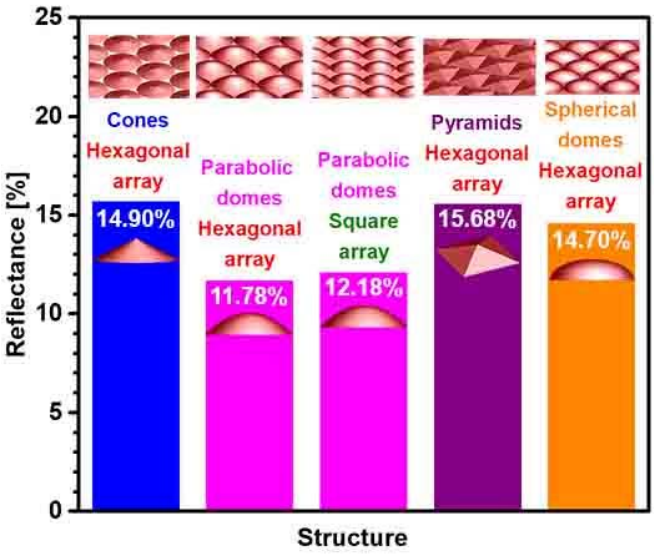

Fig. 5. The total reflectance of arrays of different structures and spatial arrangments.

B. Raman Spectroscopy

Fig. 6 compares Raman spectra of samples A and B to a reference spectrum of c-plane sapphire. The sapphire reference spectrum has five peaks located at 378, 417, 449, 576 and 750 cm^{-1}, which match published [33] values of 378, 418, 451, 578, and 751 cm^{-1}. A sixth previously reported peak at 432 cm^{-1} [33] is an unresolved shoulder in our spectrum. The MoS_2 samples A and B have Raman spectra comprising four peaks located at 283, 379, 406 and 450 cm^{-1} in agreement with earlier reports for 2H-MoS_2, which has first order Raman-active modes E_{1g}, E^1_{2g}, and A_{1g} [34]-[37]. The peaks are slightly red-shifted and broadened, as expected for polycrystalline material in comparison with single crystal [36]. It is evident from the

Raman spectra of samples A and B that the difference in growth time does not have a great effect on the quality of the as-grown MoS_2 film.

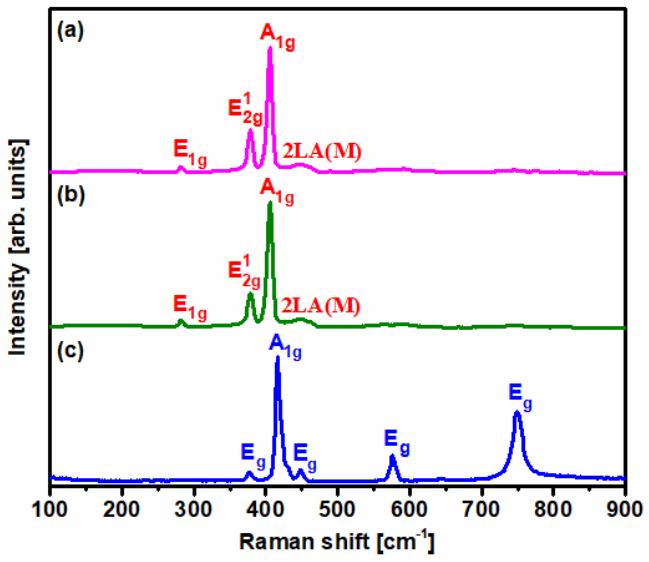

Fig. 6. Raman spectra of MoS_2-on-sapphire (a) sample A, (b) sample B, and (c) blank c-plane sapphire wafer.

C. X-ray Diffraction

Fig. 7 shows symmetric out-of-plane X-ray diffraction patterns for samples A and B of MoS_2. Six diffraction peaks of MoS_2 are identified which corresponding to the (002), (004), (100), (006), (110) and (008) planes, respectively. The location of these peaks matches well the XRD card PDF # 00-37-1492.

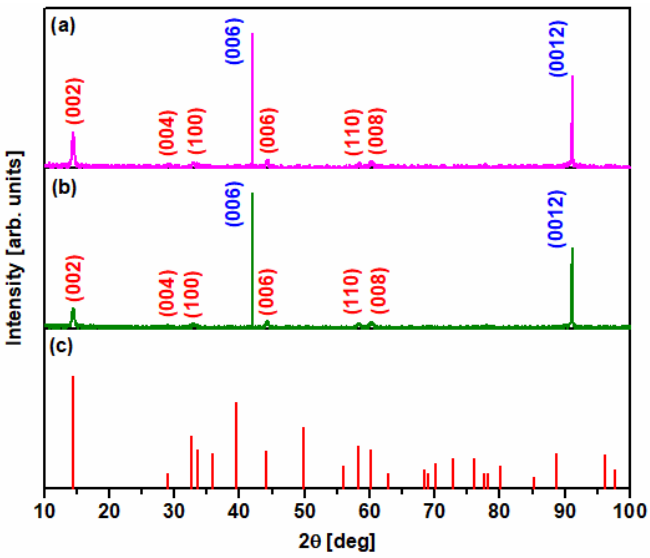

Fig. 7. Symmetric Out-of-plane XRD patterns of (a) sample A, (b) sample B and (c) reference XRD pattern of MoS_2. MoS_2 peaks are labeled in red and sapphire peaks are labeled in blue.

The presence of diffraction peaks from unparallel planes confirms the polycrystalline nature of the film. Two diffraction peaks (006) and (0 0 12) from the sapphire substrate are identified (PDF # 01-070-5679). The relative strength of the (002) peak indicates preferred orientation such that the (002) plane of MoS_2 is parallel to the (006) plane of the sapphire substrate. The polycrystalline nature according to the x-ray diffraction agrees well with Raman analysis.

D. SEM and EDX

Fig. 8a shows a SEM image of the surface of evaporated Mo thin film before sulfurization. The Mo film was smooth and dense. SEM images of the surface of sample B of MoS_2 at different magnifications are shown in Fig. 8b-d. The microdomes are randomly distributed and uniformly cover the whole surface. EDX data of sample B over an area equivalent to the field of view of Fig. 8d gives S/Mo ratio of 1.96, which indicate that the film is almost stoichiometric. A reasonable explanation of the cause of the formation of these microdomes is the small thickness of the Mo thin film and coefficient of thermal expansion mismatch between the sapphire substrate ($7.3\times10^{-6}/℃$) and the grown MoS_2 ($10.7\times10^{-6}/℃$) [38], [39].

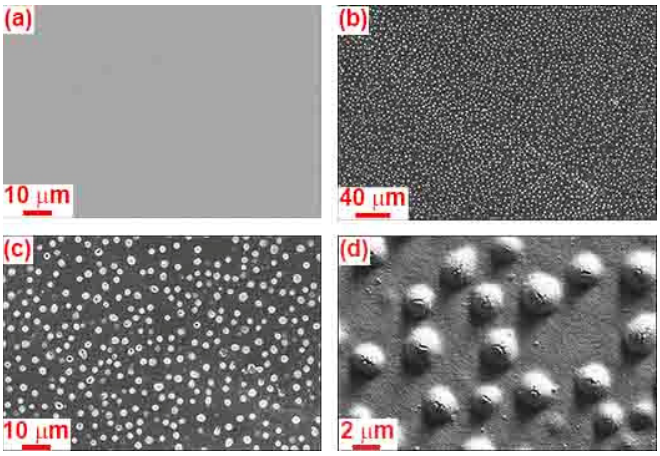

Fig. 8. SEM images of the surface of (a) Mo thin film before sulfurization (b-d) Sample B of MoS_2 at different magnifications.

E. Reflectance Measurement And Simulation

Fig. 9 compares the experimentally measured total reflectance (specular plus diffuse) spectrum of MoS_2 sample B with that simulated for a square array of parabolic domes (2 μm in diameter and 1 μm in height) with a period of 2.2 μm. The simulation of an area of a few microns requires large computing resources, therefore we chose to simulate a periodic spatial distribution with Bloch boundary condition. Although the regular distribution of simulated domes differs from the random arrangement on the actual sample, it nevertheless demonstrates a strong reduction in reflectance that agrees well with

experiment. Based on experimental measurement and simulation domes with 2 µm base diameter could reduce the reflectance by 45% which consequently improves light harvesting and solar cell efficiency.

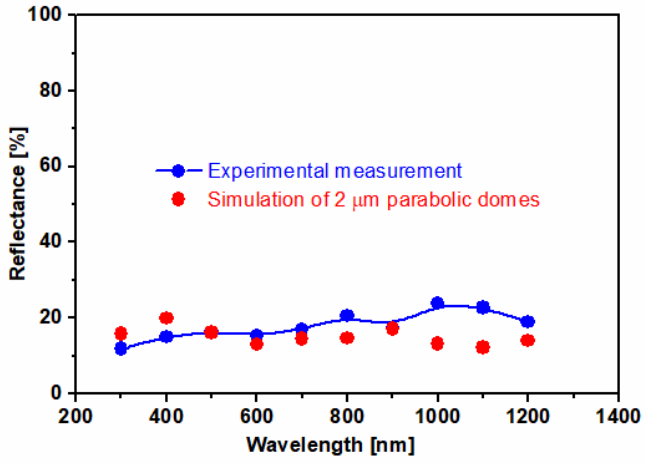

Fig. 9. The reflectance of MoS_2-on-sapphire sample B in comparison with simulation for parabolic domes with 2 µm base diameter.

V. Conclusion

Different structures and geometries have been studied and analyzed by FDTD method to assess their performance for antireflection applications. A comparison between cones, pyramids, parabolic and spherical domes of the same base area and height showed that parabolic domes are the best antireflection structures. A parabolic dome of 0.5µm base diameter and 2µm height can reduce reflectance to almost zero for all incident angles from 0° to 50°. These antireflections structures can boost MoS_2-based solar cells efficiency by almost 50%. MoS_2 films with microdome texture were grown by APCVD. SEM images revealed the uniform random distribution of these microdomes. Stoichiometric composition and structure of MoS_2 have been confirmed by EDX, Raman spectroscopy, and x-ray diffraction. Based on experimental measurement and simulation domes with 2 µm base diameter and 1 µm height could reduce the reflectance by 45%.

References

[1] S. Lien, D. Wuu, W. Yeh, and J. Liu, "Tri-layer antireflection coatings (SiO_2/SiO_2–TiO_2/TiO_2) for silicon solar cells using a sol–gel technique," *Solar Energy Materials and Solar Cells,* vol. 90, pp. 2710-2719, 2006.

[2] V. M. Aroutiounian, K. Martirosyan, and P. Soukiassian, "Almost zero reflectance of a silicon oxynitride/porous silicon double layer antireflection coating for silicon photovoltaic cells," *Journal of Physics D: Applied Physics,* vol. 39, pp. 1623-1625, 2006.

[3] D. Bouhafs, "Design and simulation of antireflection coating systems for optoelectronic devices: Application to silicon solar cells," *Solar Energy Materials and Solar Cells,* vol. 52, pp. 79-93, 1998.

[4] B. W. Schneider, N. N. Lal, S. Baker-Finch, and T. P. White, "Pyramidal surface textures for light trapping and antireflection in perovskite-on-silicon tandem solar cells," *Optics Express,* vol. 22 pp. a1422-a1430, 2014.

[5] Y. C. Wang, H. Y. Cheng, Y. T. Yen, T. T. Wu, C. H. Hsu, H. W. Tsai, C. H. Shen, J. M. Shieh, and Y. L. Chueh, "Large-scale micro- and nanopatterns of $Cu(In,Ga)Se_2$ thin film solar cells by mold-assisted chemical-etching process," *ACS Nano,* vol. 9, pp. 3907-3916, 2015.

[6] H. P. Wang, T. Y. Lin, M. L. Tsai, W. C. Tu, M. Y. Huang, C. W. Liu, Y. L. Chueh, and J. H. He, "Toward efficient and omnidirectional n-type Si solar cells: concurrent improvement in optical and electrical characteristics by employing microscale hierarchical structures," *ACS Nano,* vol. 8, pp. 2959-69, 2014.

[7] D. Iencinella, E. Centurioni, R. Rizzoli, and F. Zignani, "An optimized texturing process for silicon solar cell substrates using TMAH," *Solar Energy Materials and Solar Cells,* vol. 87, pp. 725-732, 2005.

[8] L. Han and H. Zhao, "Simulation analysis of GaN microdomes with broadband omnidirectional antireflection for concentrator photovoltaics," *Journal of Applied Physics,* vol. 115, p. 133102, 2014.

[9] M. Nam, J. Lee, and K.-K. Lee, "Efficiency improvement of solar cells by importing microdome-shaped anti-reflective structures as a surface protection layer," *Microelectronic Engineering,* vol. 88, pp. 2314-2318, 2011.

[10] R. Dewan, I. Vasilev, V. Jovanov, and D. Knipp, "Optical enhancement and losses of pyramid textured thin-film silicon solar cells," *Journal of Applied Physics,* vol. 110, p. 013101, 2011.

[11] P. Papet, O. Nichiporuk, A. Kaminski, Y. Rozier, J. Kraiem, J. F. Lelievre, A. Chaumartin, A. Fave, and M. Lemiti, "Pyramidal texturing of silicon solar cell with TMAH chemical anisotropic etching," *Solar Energy Materials and Solar Cells,* vol. 90, pp. 2319-2328, 2006.

[12] H. H. Lin, W. H. Chen, and F. C. Hong, "Improvement of polycrystalline silicon wafer solar cell efficiency by forming nanoscale pyramids on wafer surface using a self-mask etching technique," *Journal of Vacuum Science & Technology B,* vol. 31, p. 31401, 2013.

[13] S. C. Baker-Finch and K. R. McIntosh, "Reflection of normally incident light from silicon solar cells with pyramidal texture," *Progress in Photovoltaics: Research and Applications,* vol. 19, pp. 406-416, 2011.

[14] W. H. Southwell, "Pyramid-array surface-relief structures producing antireflection index matching on optical surfaces," *Journal of the Optical Society of America A,* vol. 8, pp. 549-553, 1991.

[15] R. Dewan, S. Fischer, V. B. Meyer-Rochow, Y. Ozdemir, S. Hamraz, and D. Knipp, "Studying nanostructured nipple arrays of moth eye facets helps to design better thin film solar cells," Bioinspiration and Biomimetics, vol. 7, p. 016003, 2012.

[16] J. Zhu, C. M. Hsu, Z. Yu, S. Fan, and Y. Cui, "Nanodome solar cells with efficient light management and self-cleaning," *Nano Letters,* vol. 10, pp. 1979-84, 2010.

[17] L. Yang, Q. Feng, B. Ng, X. Luo, and M. Hong, "Hybrid moth-eye structures for enhanced broadband antireflection characteristics," *Applied Physics Express,* vol. 3, p. 102602, 2010.

[18] Y. Kim, N. D. Lam, K. Kim, W. K. Park, and J. Lee, "Ge nanopillar solar cells epitaxially grown by metalorganic chemical vapor deposition," *Scientific Reports,* vol. 7, p. 42693, 2017.
[19] B. D. Choudhury and S. Anand, "Rapid thermal annealing treated spin-on doped antireflective radial junction Si nanopillar solar cell," *Optics Express,* vol. 25, pp. A200-A207, 2017.
[20] J. Proust, A. L. Fehrembach, F. Bedu, I. Ozerov, and N. Bonod, "Optimized 2D array of thin silicon pillars for efficient antireflective coatings in the visible spectrum," *Scientific Reports,* vol. 6, p. 24947, 2016.
[21] P. Spinelli, M. A. Verschuuren, and A. Polman, "Broadband omnidirectional antireflection coating based on subwavelength surface Mie resonators," *Nature communications,* vol. 3, p. 692, 2012.
[22] R. Rebigan, A. Avram, F. Craciunoiu, R. Tomescu, E. Budianu, M. Purica, and M. Popescu, "Silicon plasma processing for antireflective micro-textured surfaces with applications for solar cells," presented at the CAS 2013 (International Semiconductor Conference), Sinaia, Romania, 2013.
[23] P. B. Clapham and M. C. Hutley, "Reduction of Lens Reflexion by the "Moth Eye" Principle," *Nature,* vol. 244, pp. 281-282, 1973.
[24] C. G. Bernhard and W. H. Miller, "A corneal nipple pattern in insect compound eyes," *Acta Physiologica Scandinavica,* vol. 56, pp. 385-386, 1962.
[25] P. I. Stavroulakis, S. A. Boden, T. Johnson, and D. M. Bagnall, "Suppression of backscattered diffraction from sub-wavelength 'moth-eye' arrays," *Opt Express,* vol. 21, pp. 1-11, 2013.
[26] C.-H. Sun, P. Jiang, and B. Jiang, "Broadband moth-eye antireflection coatings on silicon," *Applied Physics Letters,* vol. 92, p. 061112, 2008.
[27] M. Shanmugam, C. A. Durcan, and B. Yu, "Layered semiconductor molybdenum disulfide nanomembrane based Schottky-barrier solar cells," *Nanoscale,* vol. 4, pp. 7399-7405, 2012.
[28] A. Jäger-Waldau, M. C. Lux-Steiner, and E. Bucher, "MoS_2, $MoSe_2$, WS_2 and WSe_2 thin films for photovoltaics," *Solid State Phenomena,* vol. 37-38, pp. 479-484, 1994.
[29] L. Britnell, R. M. Ribeiro, A. Eckmann, R. Jalil, B. D. Belle, A. Mishchenko, Y. J. Kim, R. V. Gorbachev, T. Georgiou, S. V. Morozov, A. N. Grigorenko, A. K. Geim, C. Casiraghi, A. H. Castro Neto, and K. S. Novoselov, "Strong light-matter interactions in heterostructures of atomically thin films," *Science,* vol. 340, pp. 1311-1314, 2013.
[30] Z. Yu, Y. Pan, Y. Shen, Z. Wang, Z. Y. Ong, T. Xu, R. Xin, L. Pan, B. Wang, L. Sun, J. Wang, G. Zhang, Y. W. Zhang, Y. Shi, and X. Wang, "Towards intrinsic charge transport in monolayer molybdenum disulfide by defect and interface engineering," *Nature communications,* vol. 5, p. 5290, 2014.
[31] H. Zhang, Y. Ma, Y. Wan, X. Rong, Z. Xie, W. Wang, and L. Dai, "Measuring the refractive index of highly crystalline monolayer MoS_2 with high confidence," *Scientific Reports,* vol. 5, p. 8440, 2015.
[32] T. C. Choy, *Effective medium theory principles and applications*. Oxford, United Kingdom: Oxford University Press, 2016.
[33] M. C. Munisso, W. Zhu, and G. Pezzotti, "Raman tensor analysis of sapphire single crystal and its application to define crystallographic orientation in polycrystalline alumina," *Physica Status Solidi (b): Basic Solid State Physics,* vol. 246, pp. 1893-1900, 2009.
[34] H. Li, Q. Zhang, C. C. R. Yap, B. K. Tay, T. H. T. Edwin, A. Olivier, and D. Baillargeat, "From bulk to monolayer MoS_2: evolution of Raman scattering," *Advanced Functional Materials,* vol. 22, pp. 1385-1390, 2012.
[35] A. M. Stacy and D. T. HoduL, "Raman spectra of IVB and VIB transition metal disulfides using laser energies near the absorption edges," *Journal of Physics and Chemistry of Solids,* vol. 46, pp. 405-409, 1985.
[36] G. L. Frey, R. Tenne, M. J. Matthews, M. S. Dresselhaus, and G. Dresselhaus, "Raman and resonance Raman investigation of MoS_2 nanoparticles," *physical Review B: Condensed Matter,* vol. 60, pp. 2883-2892, 1999.
[37] J. M. Chen and C. S. Wang, "Second order Raman spectrum of MoS_2 " *Solid State Communications,* vol. 14, pp. 857-860, 1974.
[38] W. M. Yim and R. J. Paff, "Thermal expansion of AlN, sapphire, and silicon," *Journal of Applied Physics,* vol. 45, pp. 1456-1457, 1974.
[39] E. M. Dudnik and V. K. Oganesyan, "Thermal expansion of some sulfides of the transition metals," *Soviet Powder Metallurgy and Metal Ceramics,* vol. 5, pp. 125-127, 1966.